6 | CO_2RR & N_2RR over Co Decorated g-C_3N_4

This chapter provides a glimpse of the reaction mechanism simulated over the Co Decorated CN (Co-CN) for CO_2RR and N_2RR. The study highlights the possible reaction intermediates formed while the reaction proceeds from CO_2 to CH_4 and N_2 to NH_3 along with the probable reaction pathways that these intermediates take. The best reducing agent among those studied in the previous chapter has been considered to understand the CO_2RR and N_2RR within the visible region of the spectrum. Gibbs free energy change and CI-NEB calculations are being proposed for future work due to computational limitations

---

6.1 Transition Metal Decorated CN

Owing to the eco-friendly nature and effectiveness in high catalytic conversion, CN a low-cost material is used for energy conversion overcoming the platinum or platinum-based materials that have dominated the field of electrocatalyst since its discovery. Recent studies on transition metal (TM) based catalysts have shown promising applications in the commercialization of photocatalysts for dye degradation, overall water splitting, hydrogen production, atmospheric carbon dioxide reduction, and nitrogen fixation. Despite high efficiency for energy conversion the carcinogenic nature of TM-based photocatalysts has reduced the interest of the scientific community around the world [160]. Single-atom catalysts (TM@Catalyst) [161], owing to their unique properties like lower oxidation state, metal-surface inter-orbital hybridization, formation of the active site, environmentally friendly nature, and large surface area with a dispersed single atom, have come as an aid to catalysts with a large concentration of TMs. Cobalt-based photocatalysts have been challenging the monopoly of platinum in active research and large-scale production for hydrogen fuel generation. The charge transfer mechanism in the Co-based catalyst shows charge facilitation to the reactive sites along with the charge dispersion over the surface increasing the surface for the catalytic reaction. Formation of the IB in the forbidden region of band structure due to TM decoration provides an advantage in terms of optical property as well as electronic property which synergistically increase the reaction kinetics. The TMs are widely utilized for doping and decoration in the CN and have reported enhancement in the visible absorption region as the narrowing of the band gap results in the redshift, while the formation of intermediate impurity states has reduced the recombination rate along with increasing charge separation as deep trap sites provide metastable state for longer lifetime for charge carriers [8, 162]. Co-doping, Co-loading, and Co-embedded heptazine-based CN system studies, both theoretical and experimental, revealed three times higher hydrogen evolution rate than pure, band gap value decrease up to 0.72 eV with an integrated electric field for recombination rate suppression,

and enhanced photoelectric property of CN with emphasis on Co(3d)-N(2p) interaction for redshift. Even though cation-doped CN has been the subject of much research, a comprehensive analysis of the function of charge transfer and how it affects the rate-determining step is still missing [8, 163].

CO_2RR, is a chemical process involving the conversion of CO_2 into valuable hydrocarbon products through the use of catalysts and electrochemical techniques. Utilization of CO_2RR shows its effect on reducing the current atmospheric pollution by its conversion into fuels like methane and methanol, whereas it provides alternate fuel solutions to the existing non-renewable energy sources. The reduction of CO_2 molecules aims to lower greenhouse gas emissions and alleviate climate change [164]. Work reported by Gao et al. [165] has shown CO_2 conversion into $HCOOH$, and CH_4 for Pd/CN, and Pt/CN with a rate-determining barrier of 0.66 eV, and 1.16 eV, respectively. To shortlist the feasible reaction mechanism over the $TM@CN$, all the possible reactions were computed over the surface with probable reaction intermediates and using the first-principles methods to check its capability for the promising application in the photo-conversion technology. Here DFT has been utilized to study the series of 3d to 5d TM loaded on CN ($TM@CN$) for CO_2 reduction [166]. Four $TM@CN$ catalysts (TM = Ni, Rh, Os, and Ir) based on a five-step screening method are used where $Rh@CN$ and $Ni@CN$ with overpotentials of -0.48 and -0.58 V, respectively [167]. The activity mechanism demonstrates that catalysts with the ideal positive charge and a negative d-band center can enhance CO_2RR performance. The atomic alteration of the CN matrix with metal atoms is the source of the high activity. Additionally, CN offers a conducive local environment for CO_2 reduction in addition to acting as a coordinating framework.

The electrochemical process known as the N_2RR produces ammonia (NH_3) from N_2 and a proton source. N_2RR is typically conducted at mild temperature and pressure, in contrast to the Haber-Bosch process, which is the standard industrial method for large-scale ammonia synthesis. Its potential to be integrated into a circuit that receives its energy supply from non-fossil sources further enhances N_2RR's appeal from an environmental standpoint [168]. The last ten years

have seen a surge in the development of electromaterials with the ability to catalyze N_2RR because NH_3 is a chemical feedstock that is primarily relevant as the source of most fertilizers. The design and development of inexpensive and effective electrocatalysts that can facilitate the N_2RR in ambient settings are essential for the production of NH_3 and offers a substitute for the conventional Harber-Bosch method [169]. For five single-atom catalysts, namely Ti, Co, Mo, W, and Pt atoms supported on CN monolayer, the Gibbs free energy change of the potential-determining step is less than that on the Ru(0001) stepped surface among all the candidates. With a limiting potential of -0.35 V via an associative enzymatic route, $W@CN$ demonstrates the greatest catalytic activity toward N_2RR and is capable of effectively suppressing the competing hydrogen evolution process. $W@CN$'s intrinsic characteristics, including its huge spin moment and considerable positive charge on the W atom, superior electrical conductivity, and moderate adsorption strength with N_2RR intermediates, are responsible for its high N_2RR activity and selectivity [170]. This study investigated the viability of using a single TM-atom (from Sc to Au) supported on $g-C_7N_3$ as π–d conjugated single-atom catalysts for N_2RR using first-principles calculations inside the density-functional theory. Hf, Ta, W, and $Re@g-C_7N_3$ were identified from 27 $TM@g-C_7N_3$ as the best $TM@CN$ for N_2RR with low limiting potentials of -0.06 to -0.46 V by a "Five-step Procedure" screening technique [171]. Another study found that when the coordination number of the single atom increases, the N_2 chemisorption activity of different single TM atoms anchored on CN with nitrogen vacancies (TM@NVCN) decreases. Even with a low coordination number, the anchoring cubic close-packed metal atom is not a favorable location for N_2 adsorption and activation. Due to the feasibility of π–d conjugated TM-CN resulting from a single TM atom anchored on $g-C_{10}N_3$ (TM = Sc–Au) for N_2RR, a single Ti atom is found to be the most promising catalyst for its excellent N_2 reduction performance, with a potential-limiting step of 0.51 eV and a rate-determining barrier of 0.57 eV [172]. The potential of $TM@CN$ for electrocatalytic reduction reactions motivates us to study these catalytic properties within the umbrella of the visible spectral region to investigate the

photocatalytic CO_2RR and N_2RR. It's not enough to specify the reactive sites or to check whether the catalyst shows the probability of CO_2/N_2 reduction but important is to understand the multiple reaction pathways that could lead to methanol (CH_3OH)/methane (CH_4) and NH_3 formation. In the present chapter, we studied the suitable reaction sites along with the reaction mechanism over $Co{-}CN$ which is reported as best photocatalyst for reduction in previous chapters.

6.2 CO_2RR and N_2RR Mechanism

Since, simulations for CO_2RR and N_2RR have been performed over the previously studied photocatalyst ($Co-CN$, Chapter 3), the computational details are similar. Electronic, optical properties in terms of DOS and $\alpha(\omega), \epsilon_2(\omega)$ will not be discussed in this part but ELF and $\Delta\rho$ will be studied for the screening of suitable sites for CO_2 and N_2 adsorption. With the adsorption of initial adsorbate CO_2 and N_2, the reduction process proceeds along the reaction intermediates whose optimized structure is shown in Fig 6.1, 6.2. CO_2 reduction takes place along the traditional eight-electron transfer procedure involving three industrial-scale fuels, $HCOH$, CH_3OH, and CH_4, possible reaction pathways are shown in Fig. 6.3. On the other hand, N_2 reduction is known to be a surface and site-selective reaction that can proceed via different mechanisms such as (i) Enzymatic, (ii) Distal, (iii) Alternating, and (iv) dissociative mechanism [173]. The given reaction intermediates, and the pathways that N_2RR follows have been illustrated in Fig. 6.4, the reaction pathways follow either Distal or alternating mechanism for NH_3 formation from N_2.

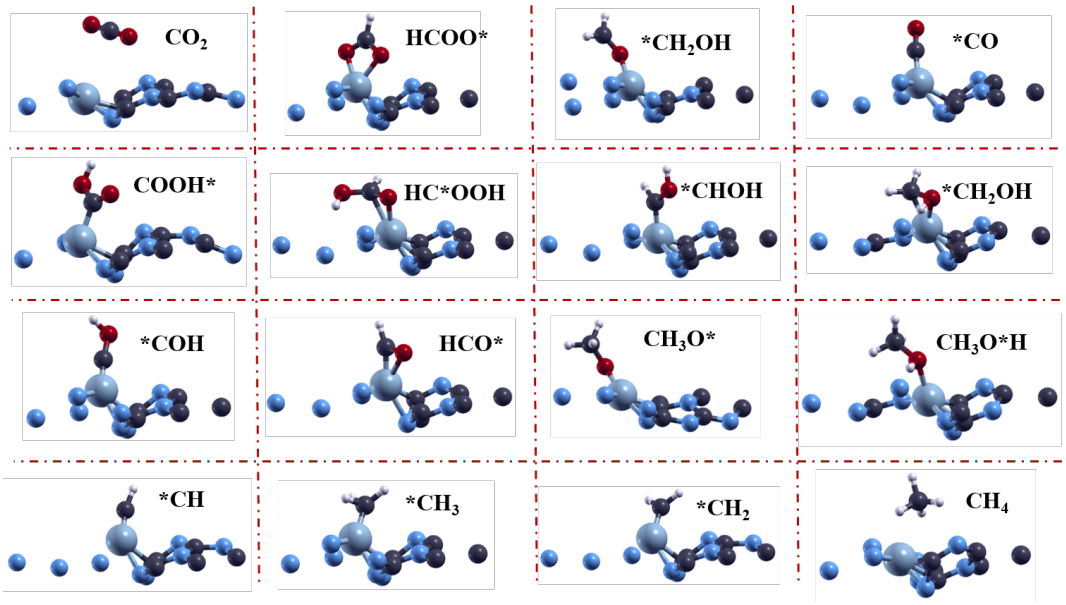

FIGURE 6.1: Possible reaction intermediates for CO_2RR over $Co-CN$.

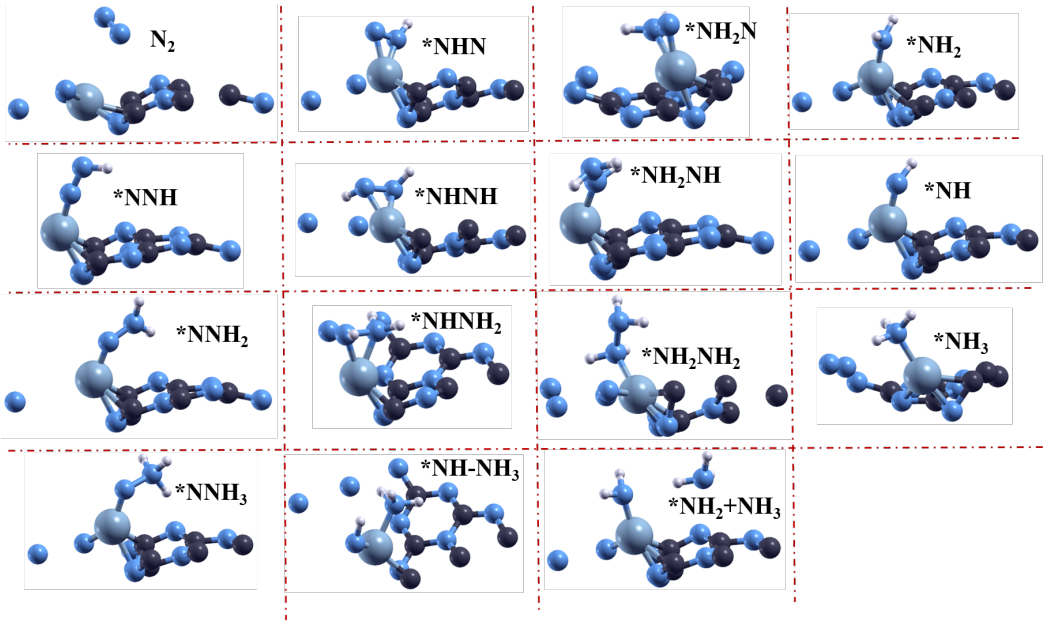

FIGURE 6.2: Possible reaction intermediates for N_2RR over $Co-CN$.

6.3 Electronic Properties and Active Site Selection

Here in this study, various sites over the surface of the CN have been selected for the Co-atom. The sites reported previously include adsorption over the N^{tri}, N^{bridge}, N^{edge}, C^{cor}, C^{bay}, hexagonal void, and, trigonal void. Where trigonal void was further studied based on the energetic stability among other existing sites. As

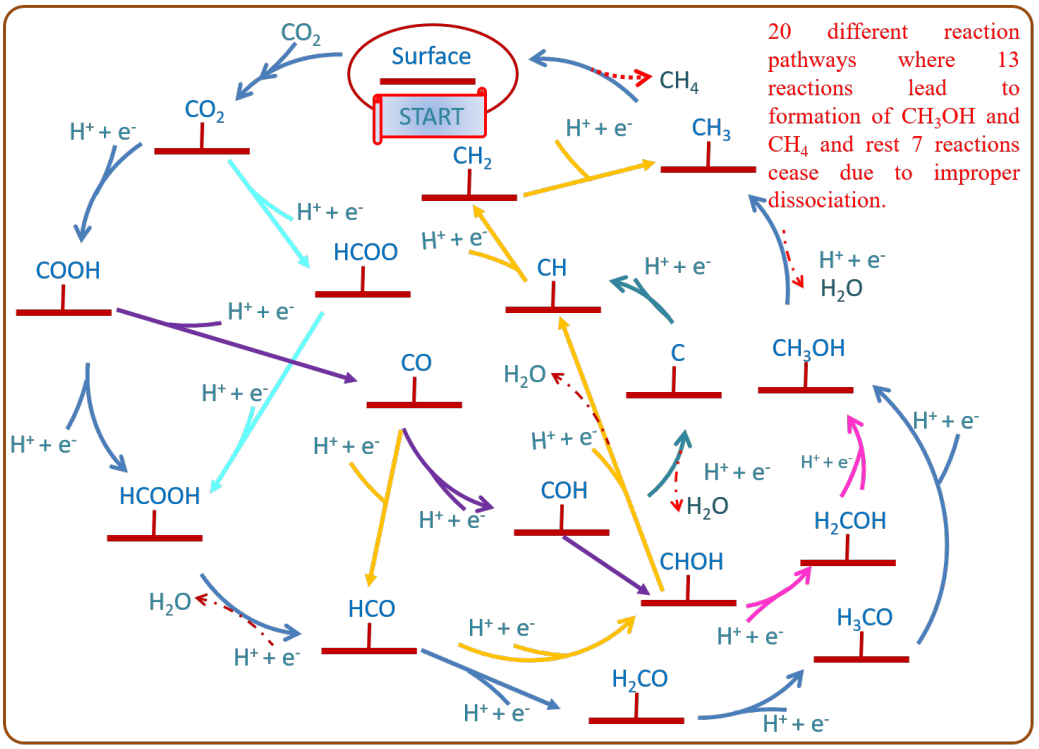

FIGURE 6.3: Reaction pathways followed of CO_2RR including the possible reaction intermediates for $Co-CN$.

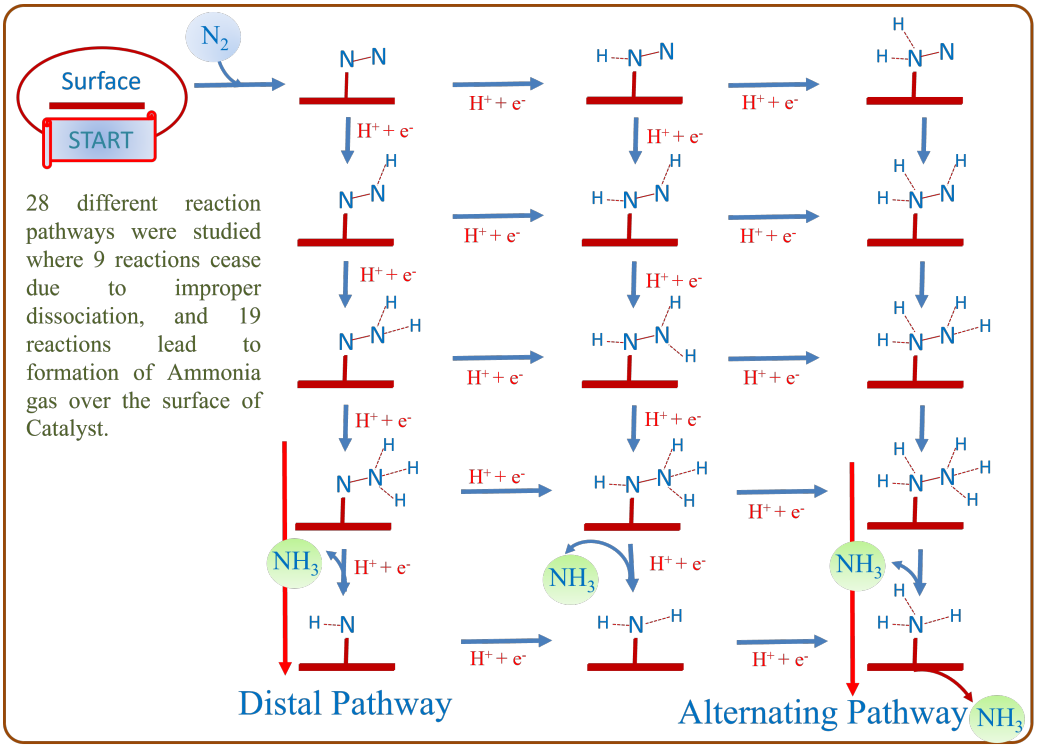

FIGURE 6.4: Reaction pathways including the Distal and alternating mechanism followed for N_2RR over $Co-CN$.

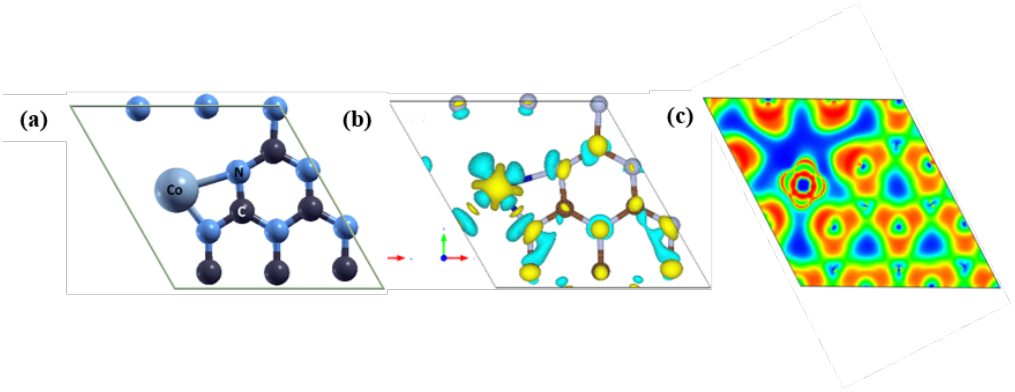

FIGURE 6.5: (a) Optimized structure, (b) Charge density difference, and (c) electron localization function plotted for $Co-CN$.

shown in Fig. 6.5, which denotes the optimized structure, $\Delta\rho$ isosurface, and ELF of $Co-CN$, Co interacts with the N^{edge} possessing a $p_\pi - d_\pi$ orbital overlap of N-2p and Co-3d orbitals, respectively. The blue region and yellow region determine the charge depletion, and charge accumulation, respectively denoting the heavy charge depletion over the interacting N-atoms. The charge depletion over the Co-N bond seen from the blue region, and charge accumulation over the surface top Co-atom, indicate the hybridization within the surface, and an increase in electron density over the Co-atom. Apart from the Co-atom, the charge increase is seen over the N^{tri}, C^{cor} atom denoting charge conjugation over the surface of the CN. ELF analysis further verifies the π-conjugation over the matrix of CN, while the charge localization over the Co- and its neighboring N-atom. The covalent bonding between the Co-N makes the region electronegative, while the lone pair of N^{edge} tending towards the Co-atom marks the region of high charge concentration. This charge variation over the $Co-CN$ surface helps to select the suitable site for electrophilic/electrophobic adsorbate to be adsorbed. The charge region denotes two specific regions, (i) the void with lone pair providing spacious charge well, and (ii) the C-N-Co-N ring formed on N-Co-N interaction which denotes a similar charge density region. Considering the adsorbate interaction over the surface, it won't be selective to the well as due to chemical interaction the adsorbate is predicted to drift towards most electronegative atoms, hence, the ring is the sweet spot for the same. Hence, we have considered two sites, Co-, and N^{edge} for the adsorption.

The formation of IB in the forbidden region of the $Co-CN$ needs to be discussed with this perspective of electronic and optical properties as this work analyzes the photocatalytic property of $Co-CN$. IB plays a two-way role in the enhancement of photoactivity of a catalyst, (i) due to the presence of the states formed due to Co-N interaction, this IB acts as a meta stable state for the electron recombination. Providing the electron an empty state and a longer lifetime to get paired with the hole present in the VB. (ii) multiple transition channels get activated creating a large number of photo-induced charge carriers efficient for long reactions such as CO_2RR and N_2RR, by providing sufficient charges for surface reactions.

6.4 CO_2RR over Co-CN

Owing to the surface site selectivity screening discussed in the previous section, CO_2 has been adsorbed over the Co, N site to check its stability. E_{ads} of -0.253, and -0.385 eV for N, and Co-site, respectively demonstrate the physisorption behavior. However, as we proceed further we see that the corresponding reaction equations are listed from Eq. 6.1- 6.20 (Eq. 6.1- 6.14 over N-site, Eq. 6.15- 6.20 over Co-site) adsorption of intermediates favors Co-atom. The possible reaction pathways followed over both the reaction sites and show potential for efficient CO_2 adsorption, and complete conversion to CH_3OH/CH_4. In total, 20 different reaction pathways were performed including, $*CO_2$, $*COOH$, $HC*OOH$, $HCOO*$, $*CO$, $HCO*$, H_2CO*, $*CHOH$, $*COH$, $*C$, $*CH$, $*CH_2$, $*CH_3$, $*CH_3O$, $*CH_2OH$ and, CH_3*OH as reaction intermediates, here the "*" represent the atom interacting with the surface as shown in Fig. 6.1(the intermediates listed here not present in figure show similar geometry for similar formula). 13 reactions among them were found to be feasible either for the formation of CH_3OH or CH_4, rest 7 reactions ceased due to improper dissociation of the reaction intermediates. Among these 20, Eq. 6.2, 6.5, 6.9, 6.15, 6.16, 6.17, and 6.18 dissociates, which may give rise to corresponding equations if multiple CO_2 molecules are considered, whereas rest all converge to CH_4

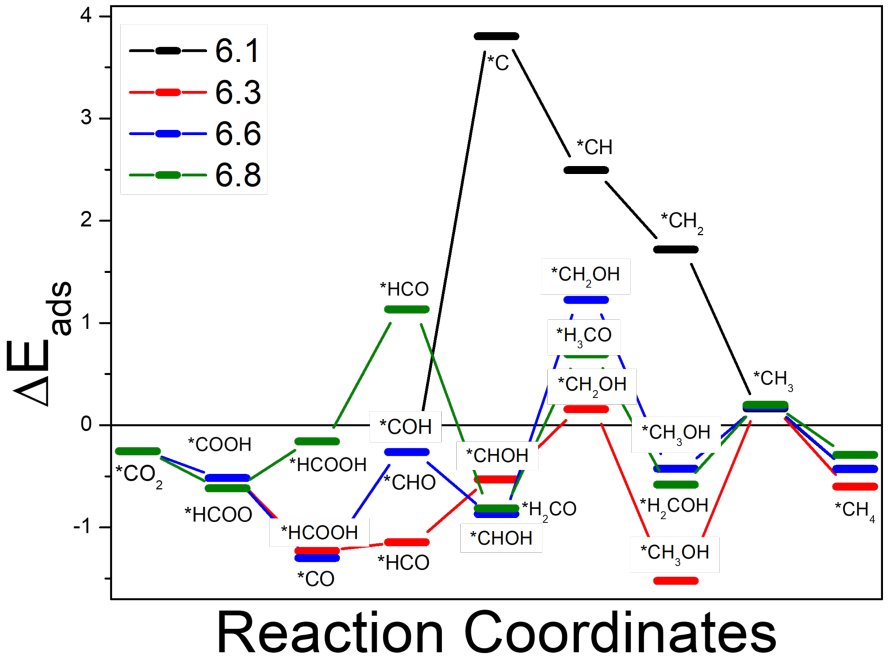

FIGURE 6.6: Distinct reaction pathways for CO_2RR over $Co-CN$.

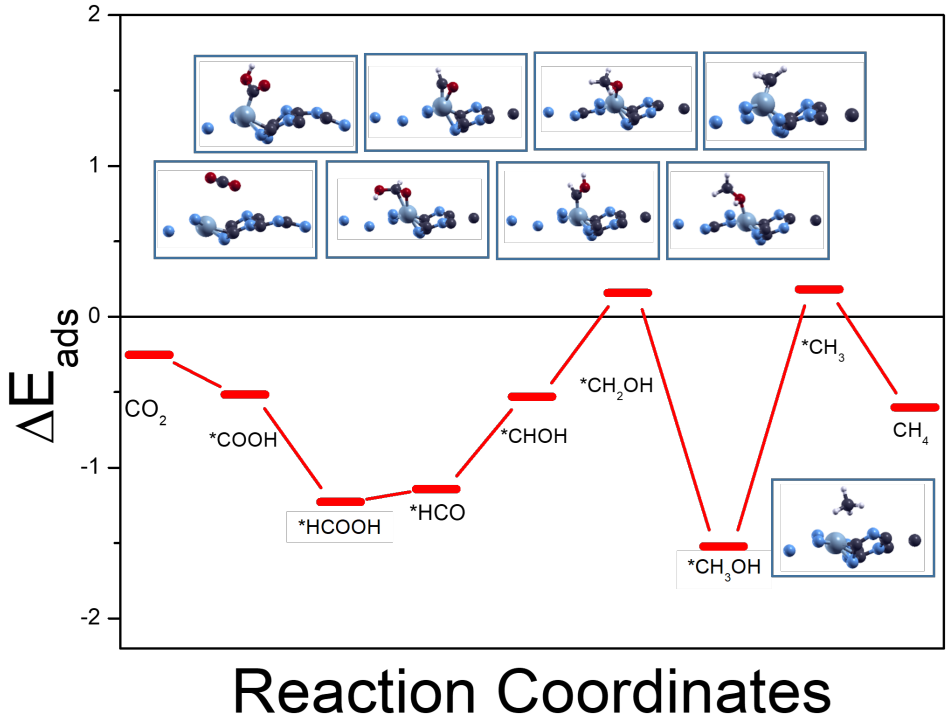

FIGURE 6.7: Most feasible reaction pathway with lowest energy barrier for CO_2RR over $Co-CN$.

$$Pristine \rightarrow *CO_2 \rightarrow *COOH \rightarrow *CO \rightarrow *COH \rightarrow *C \rightarrow *CH \rightarrow *CH_2 \rightarrow *CH_3 \rightarrow *CH_4 \quad (6.1)$$

$$Pristine \rightarrow *CO_2 \rightarrow *COOH \rightarrow *HCOOH \rightarrow *HCO \rightarrow *H_2CO \rightarrow *H_2CO + *H \quad (6.2)$$

$$Pristine \rightarrow *CO_2 \rightarrow *COOH \rightarrow *HCOOH \rightarrow *HCO \rightarrow *CHOH \rightarrow *CH_2OH \rightarrow *CH_3OH \rightarrow *CH_3 \rightarrow *CH_4 \quad (6.3)$$

$$Pristine \rightarrow *CO_2 \rightarrow *COOH \rightarrow *HCOOH \rightarrow *HCO \rightarrow *CHOH \rightarrow *CH \rightarrow *CH_2 \rightarrow *CH_3 \rightarrow *CH_4 \quad (6.4)$$

$$Pristine \rightarrow *CO_2 \rightarrow *COOH \rightarrow *CO \rightarrow *HCO \rightarrow *CO + *H \quad (6.5)$$

$$Pristine \rightarrow *CO_2 \rightarrow *COOH \rightarrow *CO \rightarrow *CHO \rightarrow *CHOH \rightarrow *CH_2OH \rightarrow *CH_3OH \rightarrow *CH_3 \rightarrow *CH_4 \quad (6.6)$$

$$Pristine \rightarrow *CO_2 \rightarrow *COOH \rightarrow *CO \rightarrow *CHO \rightarrow *CHOH \rightarrow *CH \rightarrow *CH_2 \rightarrow *CH_3 \rightarrow *CH_4 \quad (6.7)$$

$$Pristine \rightarrow *CO_2 \rightarrow *HCOO \rightarrow *HCOOH \rightarrow *HCO \rightarrow *H_2CO \rightarrow *H_3CO \rightarrow *H_3COH \rightarrow *CH_3 \rightarrow *CH_4 \quad (6.8)$$

$$Pristine \rightarrow *CO_2 \rightarrow *HCOO \rightarrow *HCOOH \rightarrow *HCO \rightarrow *CHOH \rightarrow *OCH + *H \quad (6.9)$$

$$Pristine \rightarrow *CO_2 \rightarrow *HCOO \rightarrow *HCOOH \rightarrow *HCO \rightarrow *H_2CO \rightarrow *H_3CO \rightarrow *H_3COH \rightarrow *CH_3 \rightarrow *CH_4 \quad (6.10)$$

$$Pristine \rightarrow *CO_2 \rightarrow *COOH \rightarrow *HCOOH \rightarrow *HCO \rightarrow *H_2CO \rightarrow *H_3CO \rightarrow *H_3COH \rightarrow *CH_3 \rightarrow *CH_4 \quad (6.11)$$

$$Pristine \rightarrow *CO_2 \rightarrow *COOH \rightarrow *HCOOH \rightarrow *HCO \rightarrow *CHOH \rightarrow *CH_2OH \rightarrow *CH_2 \rightarrow *CH_3 \rightarrow *CH_4 \quad (6.12)$$

$$Pristine \rightarrow *CO_2 \rightarrow *HCOO \rightarrow *HCOOH \rightarrow *HCO \rightarrow *H_2CO \rightarrow *CH_2 \rightarrow *CH_3 \rightarrow *CH_4 \quad (6.13)$$

$$Pristine \rightarrow *CO_2 \rightarrow *COOH \rightarrow *HCOOH \rightarrow *HCO \rightarrow *H_2CO \rightarrow *CH_2 \rightarrow *CH_3 \rightarrow *CH_4 \quad (6.14)$$

$$Pristine \rightarrow *CO_2 \rightarrow *COOH \rightarrow *H + *COOH \quad (6.15)$$

$$Pristine \rightarrow *CO_2 \rightarrow *HCOO \rightarrow *HCOOH \rightarrow *HCO \rightarrow *H + *CO \quad (6.16)$$

$$Pristine \rightarrow *CO_2 \rightarrow *COOH \rightarrow *CO \rightarrow *HCO \rightarrow *H + *CO \tag{6.17}$$

$$Pristine \rightarrow *CO_2 \rightarrow *COOH \rightarrow *CO \rightarrow *COH \rightarrow *CHOH \rightarrow *CH_2OH \rightarrow *CHOH + *H \tag{6.18}$$

$$Pristine \rightarrow *CO_2 \rightarrow *COOH \rightarrow *CO \rightarrow *COH \rightarrow *CHOH \rightarrow *CH \rightarrow *CH_2 \rightarrow *CH_3 \rightarrow *CH_4 \tag{6.19}$$

$$Pristine \rightarrow *CO_2 \rightarrow *COOH \rightarrow *CO \rightarrow *COH \rightarrow *C \rightarrow *CH \rightarrow *CH_2 \rightarrow *CH_3 \rightarrow *CH_4 \tag{6.20}$$

As demonstrated from Eqs. 6.1- 6.20, we can categorize the mechanism into two parts, (i) the reaction mechanism takes place with $*CH_3OH$ as an intermediate, on the other hand (ii) CO_2RR proceeds via formation of $*C$. Four reactions, owing to their different pathways are shown and plotted from Eqs. 6.1, 6.2, 6.4, 6.6 in Fig. 6.6 performed over N site. Since the N-site shows the highest probability of CO_2RR, CO_2 adsorption is preferred over the N site as compared to the Co site. However, for the Co site, CO_2RR prefers $*C$ as intermediate, while for the N site, $*CHOH$ formation pathway is preferred. This discrimination is due to the electrophilicity of the respective intermediate molecule and their interaction with the adsorption site. Fig. 6.6 represents the absorption energy vs Reaction coordinate plot, indicating the energy difference between different reaction steps, these differences represent the endothermic, and exothermic nature of the reaction step, here the downward slope shows the exothermic and feasible reaction, whereas the upwards denotes endothermic reaction. Among the plotted reactions, 4.06, 1.67. 2.08, and 1.94 eV energy differences have been shown for $*C$, $*CH_2OH$, $*CH_2OH$, and $*H_2CO$ for respective equations. Eq. 6.3, shows the lowest energy difference between the reaction's intermediate and exothermic nature for the formation of CH_3OH. The presence of multiple reaction pathways possibility, low value of change of adsorption energy, and band edges crossing the reduction potential, and similar Gibbs free energy change demonstrated by Nandha et. al.[174] concludes that CO_2 will be easily adsorbed over the surface and feasibly reduced into commercial fuels as future of energy by $Co - CN$.

6.5 N_2RR over Co-CN

To verify the stability of the N_2 adsorption over Co, N site, N_2 has been adsorbed onto it showing -0.24 and -1.45 eV E_{ads} for N and Co-site, respectively. On one hand, E_{ads} value for N-site displays moderate physisorption whereas on the other strong chemisorption of Co-site is seen. The adsorption screens and implies the role of electrophilicity over the reactive atom site, and further governs the role of complete N_2RR owing to the strong interaction between the adsorbate and adsorbent. It becomes clear that N-atom is favored by the adsorption, as the Co(d_π)-N(p_π) interaction plays a pivotal role in charge transfer which favors physisorption of N_2 over N-site and chemisorption over Co-site. The proposed reaction routes indicate the possibility of full conversion to NH_3 and efficient N_2 adsorption across both reaction sites demonstrating the role of protonation. Twenty-eight distinct reaction paths were carried out in all, including $*N_2$, $*NNH$, $*NHN$, $*NHNH$, $*NH_2NH$, $*NH_3NH$, $*NHNH_2$, $*NHNH_3$, $*NH$, $*NH_2$, $*NNH_2$, $*NNH_3$, and $*NH_3$ as chemical intermediates; as seen in Fig. 6.2. According to the Distal reaction mechanism the reaction intermediate $*N$ is formed after the dissociation of NH_3 from $*NNH_3$, but in our case, we have considered it similar to $*N + NH_3$ forms on protonation of $*NNH_3$ intermediate. The intermediates not shown in the illustrations are similar in terms of structural formule. Each reaction (Eq. 6.21-6.28 over Co-site, Eq. 6.29- 6.39 at N-site) owing to its unique bonding trends can either proceed individually or in combination. Out of these, 19 reactions are listed due to similar trends followed by excluded reactions. The large number of reaction intermediates and their possible pathways display the complex nature of N_2RR despite its five-step procedure. This complexity can be verified as among 19 reactions shown 10 reactions successfully led to the formation of NH_3 production. The remaining 7 reactions ceased as the reaction intermediates were not properly dissociated. Out of these 19, Eqs. 6.23, 6.24, 6.27, 6.28, 6.32, 6.33, 6.36, 6.38, and 6.39 dissociate and, if multiple N_2 molecules are taken into consideration,

may give rise to corresponding equations and provide complete N_2 fixation.

$$Pristine \rightarrow *N_2 \rightarrow *NNH \rightarrow *NNH_2 \rightarrow *NNH_3 \rightarrow *NH \rightarrow *NH_2 \rightarrow *NH_3 \quad (6.21)$$

$$Pristine \rightarrow *N_2 \rightarrow *NNH \rightarrow *NHNH \rightarrow *NHNH_2 \rightarrow *NHNH_3 \rightarrow *NH_2 \rightarrow *NH_3 \quad (6.22)$$

$$Pristine \rightarrow *N_2 \rightarrow *NNH \rightarrow *NHNH \rightarrow *NHNH_2 \rightarrow *NH_2NH_2 \rightarrow *NH_2NH_3 \rightarrow *NHNH_2 + 2*H \quad (6.23)$$

$$Pristine \rightarrow *N_2 \rightarrow *NNH \rightarrow *NHNH \rightarrow *NHNH_2 \rightarrow *NH_2NH_2 \rightarrow *NH_3NH_2 \rightarrow *NH_2 + *NH_2 + *H \quad (6.24)$$

$$Pristine \rightarrow *N_2 \rightarrow *NNH \rightarrow *NNH_2 \rightarrow *NHNH_2 \rightarrow *NHNH_3 \rightarrow *NH_2 \rightarrow *NH_3 \quad (6.25)$$

$$Pristine \rightarrow *N_2 \rightarrow *NNH \rightarrow *NNH_2 \rightarrow *NHNH_2 \rightarrow *NH_2NH_2 \rightarrow *NH_3NH_2 \rightarrow *NH_3 \quad (6.26)$$

$$Pristine \rightarrow *N_2 \rightarrow *NNH \rightarrow *N_2 + *H \quad (6.27)$$

$$Pristine \rightarrow *N_2 \rightarrow *NNH \rightarrow *NHNH \rightarrow *NH_2NH \rightarrow *NHNH + *H \quad (6.28)$$

$$Pristine \rightarrow *N_2 \rightarrow *NNH \rightarrow *NNH_2 \rightarrow *NNH_3 \rightarrow *NH \rightarrow *NH_2 \rightarrow *NH_3 \quad (6.29)$$

$$Pristine \rightarrow *N_2 \rightarrow *NHN \rightarrow *NHNH \rightarrow *NHNH_2 \rightarrow *NHNH_3 \rightarrow *NH_2 \rightarrow *NH_3 \quad (6.30)$$

$$Pristine \rightarrow *N_2 \rightarrow *NNH \rightarrow *NHNH \rightarrow *NHNH_2 \rightarrow *NHNH_3 \rightarrow *NH_2 \rightarrow *NH_3 \quad (6.31)$$

$$Pristine \rightarrow *N_2 \rightarrow *NNH \rightarrow *NHNH \rightarrow *NH_2NH \rightarrow *NHNH + *H \quad (6.32)$$

$$Pristine \rightarrow *N_2 \rightarrow *NNH \rightarrow *NHNH_2 \rightarrow *NH_2NH_2 \rightarrow *NH_2NH_3 \rightarrow *NH_2NH_2 + *H \quad (6.33)$$

$$Pristine \rightarrow *N_2 \rightarrow *NHN \rightarrow *NH_2N \rightarrow *NH_2NH \rightarrow *NH_2NH_2 \rightarrow *NH_2 \rightarrow *NH_3 \quad (6.34)$$

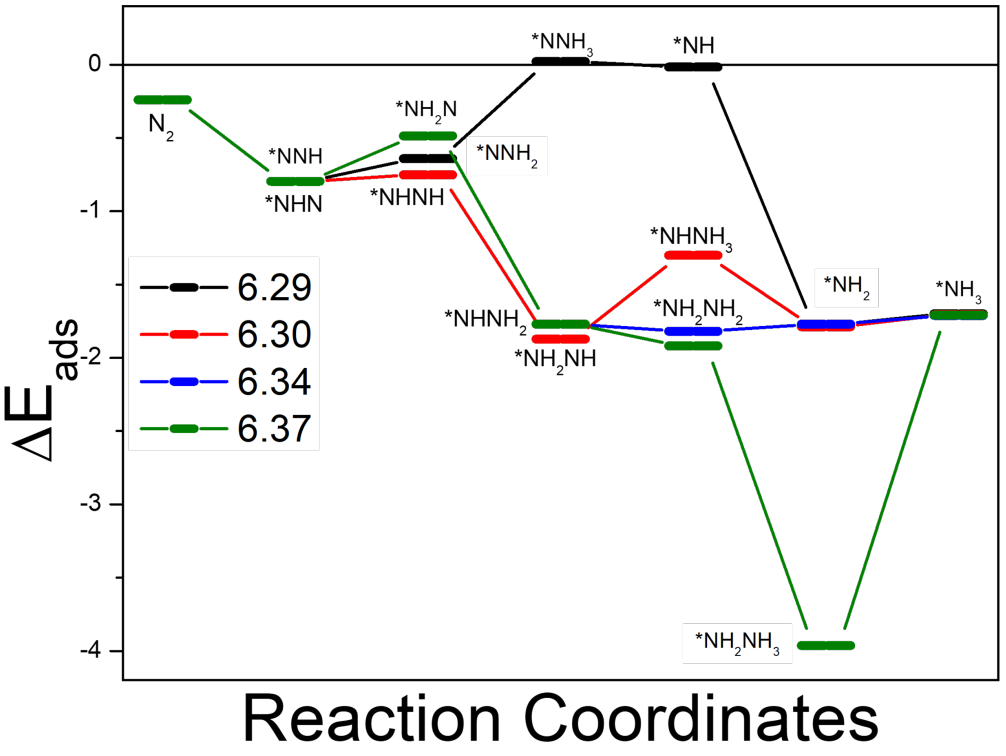

FIGURE 6.8: Distinct reaction pathways for N_2RR over $Co-CN$.

$$Pristine \rightarrow *N_2 \rightarrow *NHN \rightarrow *NHNH \rightarrow *NH_2NH \tag{6.35}$$
$$\rightarrow *NH_2NH_2 \rightarrow *NH_2NH_3 \rightarrow *NH_3$$
$$Pristine \rightarrow *N_2 \rightarrow *NHN \rightarrow *NHNH \rightarrow *NH_2NH \tag{6.36}$$
$$\rightarrow *NH_3NH \rightarrow *NH_2 + *NH_2$$
$$Pristine \rightarrow *N_2 \rightarrow *NHN \rightarrow *NH_2N \rightarrow *NH_2NH \rightarrow *NH_2NH_2 \tag{6.37}$$
$$\rightarrow *NH_2NH_3 \rightarrow *NH_3$$
$$Pristine \rightarrow *N_2 \rightarrow *NHN \rightarrow *NH_2N \rightarrow *NH_2NH \rightarrow *NH_2NH_2 \tag{6.38}$$
$$\rightarrow *NH_3NH_2 \rightarrow *NH_2NH_2 + *H$$
$$Pristine \rightarrow *N_2 \rightarrow *NNH \rightarrow *NNH_2 \rightarrow *NHNH_2 \rightarrow *NH_2NH_2 \tag{6.39}$$
$$\rightarrow *NH_3NH_2 \rightarrow *NH_2NH_2 + *H$$

As shown by Eqs. 6.21-6.39, the whole N_2RR follows either Alternating or Distal mechanism, where the former shows the alternate protonation over the non-interacting and interacting N, and later shows protonation first over the non-interacting N and then over interacting N. Meanwhile, in our case, the electronegativity of Co-forces intermediates to be adsorbed in the interacting configuration

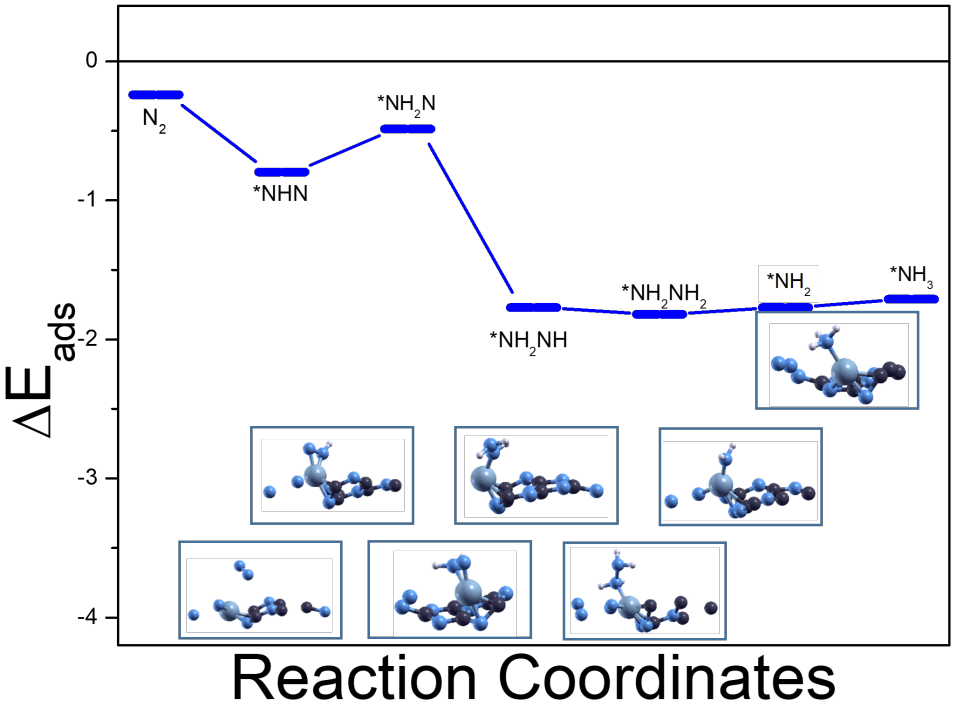

FIGURE 6.9: Most feasible reaction pathway with lowest energy barrier for N_2RR over $N-CN$.

of enzymatic mechanism, which shows simultaneous interaction of both N atoms over Co-atom. Considering these discussed categorizations we have displayed four distinct reaction mechanisms in Fig. 6.8 following Eqs. 6.29, 6.30, 6.34, and 6.37, executed ver N site. The N-site is chosen over the Co-site because it has the highest chance of N_RR and N_2 adsorption. On the other hand, the alternating mechanism of N_2RR favors the Co site and the distal route for the N site. The electrophilicity of each intermediate molecule and its interaction with the adsorption site cause this selectivity. The absorption energy vs. Reaction coordinate plot in Fig. 6.8 illustrates the energy differences between various reaction steps, signifying the endothermic and exothermic nature of the reaction step. The displayed reactions exhibit the highest energy differences of 0.66, 0.57, 0.31, and 2.26 eV for Eqs. 6.29, 6.30, 6.34, and 6.37, respectively. This highest energy difference makes them the reaction barrier with a downward reaction showing the feasibility leading to an exothermic nature. Therefore with 0.31 eV Eq. 6.34, which follows the alternating mechanism is the best suitable reaction mechanism.

The role of single-atom catalyst, $Co-CN$, for the stability of the intermediates over the reactive sites, electronegativity difference providing multiple reaction sites, π-conjugation over the surface providing feasibility in the reaction procession, the barrier height within the E_{CB}, high absorbance in the visible region of spectrum, promise the potential of $Co-CN$ as an efficient electro/photo-catalyst.

6.6 Conclusions

Co-based CN show brilliant charge transfer dynamics owing to the $p_\pi - d_\pi$ interaction of N and Co atom facilitating the charge migration axially and spatially. Wide forbidden gap prepares existing material to absorb a large number of photons resulting in equally large photo-generated charge carriers hence efficient for photo-conversion of solar energy. The presence of π-conjugation and IB provide $Co-CN$ large adsorption sites for CO_2 and N_2 reduction, high adsorption in the visible region of the spectrum, and reduced rate of recombination of photo-generated charge carriers. Potential adsorption energy value in physisorption and low difference of the adsorption energy for reaction steps display $Co-CN$ as a potential photocatalyst for efficient CO_2RR/N_2RR. However, the computation of Gibbs free energy for CO_2RR and N_2RR is not considered in the present thesis due to computational limitations.